A WELL-BALANCED RECONSTRUCTION FOR WETTING/DRYING FRONTS

ANDREAS BOLLERMANN*, ALEXANDER KURGANOV †, AND SEBASTIAN NOELLE†

Abstract. A good numerical method for the Saint-Venant system of shallow water equations must be well-balanced in the sense that the method should exactly preserve "lake at rest" steady states. There are many numerical methods capable of achieving this goal, but only in the case of submerged bottom topography. When dry areas (island, shores) are contained in the computational domain, most of well-balanced schemes fail to preserve "lake at rest" steady states unless the computational grid is adjusted to the wetting/drying fronts.

This difficulty can be overcome using a special reconstruction, which is presented in this paper. The proposed reconstruction is conservative, well-balanced and positivity preserving. We realize the new reconstruction in the framework of the second-order semi-discrete central-upwind scheme from (A. Kurganov and G. Petrova, *Commun. Math. Sci.*, 2007). The positivity of the computed water height is ensured following (A. Bollermann, S. Noelle and M. Lukáčová, *Commun. Comput. Phys.*, 2010): The outgoing fluxes are limited in case of draining cells.

Key words. Hyperbolic systems of conservation and balance laws, Saint-Venant system of shallow water equations, finite volume methods, well-balanced schemes.

AMS subject classifications. 76M12, 35L65

1. Introduction

We study numerical methods for the Saint-Venant system of shallow water equations [22], which is widely used for the flow of water in rivers or in the ocean. In one dimension, the Saint-Venant system reads:

$$\begin{cases} h_t+(hu)_x=0, \\ (hu)_t+\left(hu^2+\dfrac{1}{2}gh^2\right)_x=-ghB_x, \end{cases} \tag{1.1}$$

subject to the initial conditions

$$h(x,0)=h_0(x), \quad u(x,0)=u_0(x),$$

where $h(x,t)$ is the fluid depth, $u(x,t)$ is the velocity, g is the gravitational constant, and the function $B(x)$ represents the bottom topography, which is assumed to be independent of time t. The systems (1.1) is considered in a certain spatial domain X and if $X\neq\mathbb{R}$ the Saint-Venant system must be augmented with proper boundary conditions.

In many applications, quasi steady solutions of the system (1.1) are to be captured using a (practically affordable) coarse grid. In such a situation, small perturbations of steady states may be amplified by the scheme and the so-called numerical storm can spontaneously develop. To prevent it, one has to develop a well-balanced scheme—a scheme that is capable of exactly balancing the flux and source terms so that "lake at rest" steady states,

$$u=0, \quad w:=h+B=\text{Const.} \tag{1.2}$$

*IGPM, RWTH Aachen, Templergraben 55, 52062 Aachen, Germany.

†Mathematics Department, Tulane University, New Orleans, LA 70118, (kurganov@math.tulane.edu).

are preserved within the machine accuracy. Here, w denotes the total water height or *free surface*. Examples of such schemes can be found in [1, 2, 3, 6, 7, 9, 11, 13, 14, 17, 18, 19, 20, 21, 27, 28].

Another difficulty one often has to face in practice is related to the presence of dry areas (island, shore) in the computational domain. As the eigenvalues of the Jacobian of the fluxes in (1.1) are $u\pm\sqrt{gh}$, the system (1.1) will not be strictly hyperbolic in the dry areas ($h=0$), and if due to numerical oscillations h becomes negative, the calculation will simply break down. It is thus crucial for a good scheme to preserve the positivity of h (positivity preserving schemes can be found, e.g., in [1, 2, 9, 11, 18, 19]).

We would also like to point out that when $h=0$ the "lake at rest" steady state (1.2) reduces to

$$hu=0,\quad h=0, \tag{1.3}$$

which can be viewed as a "dry lake". A good numerical scheme may be considered "truly" well-balanced when it is capable of exactly preserving both "lake at rest" and "dry lake" steady states, as well as their combinations corresponding to the situations, in which the domain X is split into two nonoverlapping parts X_1 (wet area) and X_2 (dry area) and the solution satisfies (1.2) in X_1 and (1.3) in X_2.

We focus on Godunov-type schemes, in which a numerical solution realized at a certain time level by a global (in space) piecewise polynomial reconstruction, is evolved to the next time level using the integral form of the system of balance laws. In order to design a well-balanced scheme for (1.1), it is necessary that this reconstruction respects both the "lake at rest" (1.2) and "dry lake" (1.3) steady-state solutions as well as their combinations. On the other hand, to preserve positivity we have to make sure that the reconstruction preserves a positive water height for all reconstructed values. In this paper, we propose a piecewise linear reconstruction that satisfies the above properties. The new reconstruction is based on the proper discretization of a front cell in the situation like the one depicted in Figure 1.1. The left picture depicts the real situation with a sloping shore, while on the right we see a discretization of the same situation that seems to be the most suitable from a numerical perspective. We also demonstrate that the correct handling of (1.2), (1.3) and their combinations leads to a proper treatment of non-steady states as well.

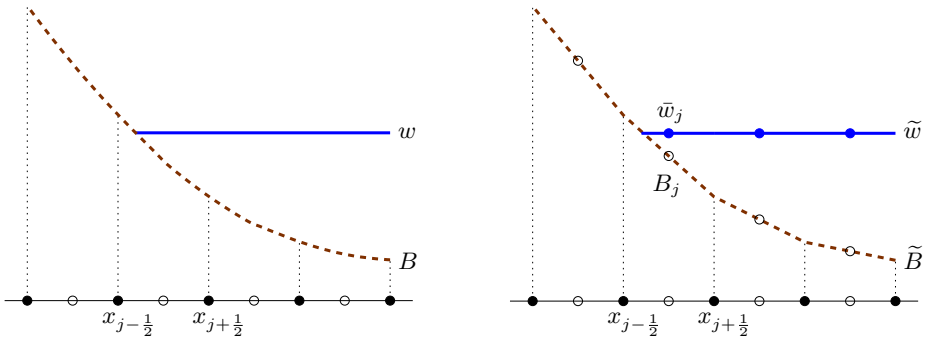

FIG. 1.1. "Lake at rest" steady state combined with dry boundaries. Left: Real situation. Right: Discretization with the desired reconstruction.

Provided the reconstruction preserves positivity, we can prove that the resulting central-upwind scheme is positivity preserving. In fact, the proof from [11] carries

over to the new scheme, but with a possibly severe time step constraint. We therefore adopt the ideas from [2] and limit outgoing fluxes whenever the so-called local draining time is smaller than the global time step. This approach ensures positive water heights without a reduction of the global time step.

The paper is organized as follows. In §2, we briefly review the well-balanced positivity preserving central-upwind scheme from [11]. A new positivity preserving reconstruction is presented in §3. The well-balancing and positivity preserving properties properties of the new scheme are proven in §4. Finally, we demonstrate a superb performance of the proposed method in §5.

2. A Central-Upwind Scheme for the Shallow Water Equations

Our work will be based on the central-upwind scheme proposed in [11]. We will therefore begin with a brief overviews of the original scheme.

We introduce a uniform grid $x_\alpha := \alpha\Delta x$, with finite volume cells $I_j := [x_{j-\frac{1}{2}}, x_{j+\frac{1}{2}}]$ of length Δx ad denote by $\overline{\mathbf{U}}_j(t)$ the cell averages of the solution $\mathbf{U} := (w, hu)^T$ of (1.1) computed at time t:

$$\overline{\mathbf{U}}_j(t) \approx \frac{1}{\Delta x}\int\limits_{I_j} \mathbf{U}(x,t)\,dx. \tag{2.1}$$

We then replace the bottom function B with its continuous, piecewise linear approximation $\widetilde{B}$. To this end, we first define

$$B_{j+\frac{1}{2}} := \frac{B(x_{j+\frac{1}{2}}+0)+B(x_{j+\frac{1}{2}}-0)}{2}, \tag{2.2}$$

which in case of a continuous function B reduces to $B_{j+\frac{1}{2}} = B(x_{j+\frac{1}{2}})$, and then interpolate between these points to obtain

$$\widetilde{B}(x) = B_{j-\frac{1}{2}} + \left(B_{j+\frac{1}{2}} - B_{j-\frac{1}{2}}\right)\cdot\frac{x-x_{j-\frac{1}{2}}}{\Delta x}, \quad x_{j-\frac{1}{2}} \le x \le x_{j+\frac{1}{2}}. \tag{2.3}$$

From (2.3), we obviously have

$$B_j := \widetilde{B}(x_j) = \frac{1}{\Delta x}\int\limits_{I_j}\widetilde{B}(x)\,dx = \frac{B_{j+\frac{1}{2}}+B_{j-\frac{1}{2}}}{2}. \tag{2.4}$$

The central-upwind semi-discretization of (1.1) can be written as the following system of time-dependent ODEs:

$$\frac{d}{dt}\overline{\mathbf{U}}_j(t) = -\frac{\mathbf{H}_{j+\frac{1}{2}}(t)-\mathbf{H}_{j-\frac{1}{2}}(t)}{\Delta x} + \overline{\mathbf{S}}_j(t), \tag{2.5}$$

where $\mathbf{H}_{j+\frac{1}{2}}$ are the central-upwind numerical fluxes and $\overline{\mathbf{S}}_j$ is an appropriate discretization of the cell averages of the source term:

$$\overline{\mathbf{S}}_j(t) \approx \frac{1}{\Delta x}\int\limits_{I_j}\mathbf{S}(\mathbf{U}(x,t),B(x))\,dx, \quad \mathbf{S} := (0, -ghB_x)^T. \tag{2.6}$$

Using the definitions (2.2) and (2.4), we write the second component of the discretized source term (2.6) as (see [9] and [11] for details)

$$\overline{\mathbf{S}}^{(2)}_j(t) \approx -g\overline{h}_j\frac{B_{j+\frac{1}{2}}-B_{j-\frac{1}{2}}}{\Delta x}. \tag{2.7}$$

The central-upwind numerical fluxes $\mathbf{H}_{j+\frac{1}{2}}$ are given by:

$$\mathbf{H}_{j+\frac{1}{2}}(t)=\frac{a^+_{j+\frac{1}{2}}\mathbf{F}(\mathbf{U}^-_{j+\frac{1}{2}},B_{j+\frac{1}{2}})-a^-_{j+\frac{1}{2}}\mathbf{F}(\mathbf{U}^+_{j+\frac{1}{2}},B_{j+\frac{1}{2}})}{a^+_{j+\frac{1}{2}}-a^-_{j+\frac{1}{2}}}$$
$$+\frac{a^+_{j+\frac{1}{2}}a^-_{j+\frac{1}{2}}}{a^+_{j+\frac{1}{2}}-a^-_{j+\frac{1}{2}}}\Big[\mathbf{U}^+_{j+\frac{1}{2}}-\mathbf{U}^-_{j+\frac{1}{2}}\Big], \tag{2.8}$$

where we use the following flux notation:

$$\mathbf{F}(\mathbf{U},B):=\left(hu,\frac{(hu)^2}{w-B}+\frac{g}{2}(w-B)^2\right)^T. \tag{2.9}$$

The values $\mathbf{U}^\pm_{j+\frac{1}{2}}$ represent the left and right values of the solution at point $x_{j+\frac{1}{2}}$ obtained by a piecewise linear reconstruction

$$\widetilde{\mathbf{U}}(x):=\overline{\mathbf{U}}_j+(\mathbf{U}_x)_j(x-x_j),\quad x_{j-\frac{1}{2}}<x<x_{j+\frac{1}{2}}, \tag{2.10}$$

of $\mathbf{U}$. This reconstruction will be second-order accurate if the approximate values of the derivatives $(\mathbf{U}_x)_j\equiv((w_x)_j,((hu)_x)_j)^T$ are at least first-order approximations of the corresponding exact derivatives. To ensure a non-oscillatory nature of the reconstruction (2.10) and thus to avoid spurious oscillations in the numerical solution, one has to evaluate $(\mathbf{U}_x)_j$ using a nonlinear limiter. From the large selection of the limiters readily available in the literature (see, e.g., [4, 8, 12, 14, 15, 16, 23]), we chose the generalized minmod limiter ([12, 15, 16, 23]):

$$(\mathbf{U}_x)_j=\text{minmod}\left(\theta\frac{\overline{\mathbf{U}}_j-\overline{\mathbf{U}}_{j-1}}{\Delta x},\frac{\overline{\mathbf{U}}_{j+1}-\overline{\mathbf{U}}_{j-1}}{2\Delta x},\theta\frac{\overline{\mathbf{U}}_{j+1}-\overline{\mathbf{U}}_j}{\Delta x}\right),\quad \theta\in[1,2], \tag{2.11}$$

where the minmod function, defined as

$$\text{minmod}(z_1,z_2,...):=\begin{cases}\min_j\{z_j\}, & \text{if } z_j>0\ \ \forall j,\\ \max_j\{z_j\}, & \text{if } z_j<0\ \ \forall j,\\ 0, & \text{otherwise,}\end{cases} \tag{2.12}$$

is applied in a componentwise manner, and θ is a parameter affecting the numerical viscosity of the scheme. It is shown in [11] that this procedure (as well as any alternative "conventional" reconstruction, including the simplest first-order piecewise constant one, for which $(\mathbf{U}_x)_j\equiv\mathbf{0}$) might produce negative values $h^\pm_{j+\frac{1}{2}}$ near the dry areas (see [11]). Therefore, the reconstruction (2.10)–(2.12) must be corrected there. The correction algorithm used in [11] restores positivity of the reconstruction, but destroys the well-balancing property. This is explained in §3, where we propose an alternative positivity preserving reconstruction, which is capable of exactly preserving the "lake at rest" and the "dry lake" steady states as well as their combinations.

Finally, the local speeds $a^\pm_{j+\frac{1}{2}}$ in (2.8) are obtained using the eigenvalues of the Jacobian $\frac{\partial\mathbf{F}}{\partial\mathbf{U}}$ as follows:

$$a^+_{j+\frac{1}{2}}=\max\left\{u^+_{j+\frac{1}{2}}+\sqrt{gh^+_{j+\frac{1}{2}}},u^-_{j+\frac{1}{2}}+\sqrt{gh^-_{j+\frac{1}{2}}},0\right\}, \tag{2.13}$$

$$a^-_{j+\frac{1}{2}}=\min\left\{u^+_{j+\frac{1}{2}}-\sqrt{gh^+_{j+\frac{1}{2}}},u^-_{j+\frac{1}{2}}-\sqrt{gh^-_{j+\frac{1}{2}}},0\right\}. \tag{2.14}$$

Note that for $\overline{\mathbf{U}}_j$, $\mathbf{U}^{\pm}_{j+\frac{1}{2}}$ and $a^{\pm}_{j+\frac{1}{2}}$, we dropped the dependence of t for simplicity.

As in [11], in our numerical experiments, we use the third-order strong stability preserving Runge-Kutta (SSP-RK) ODE solver (see [5] for details) to numerically integrate the ODE system (2.5).

3. A New Reconstruction at the Almost Dry Cells

In the presence of dry areas, the central-upwind scheme described in the previous section may create negative water depth values at the reconstruction stage. To understand this, one may look at Figure 3.1, where we illustrate the following situation: The solution satisfies (1.2) for $x>x^\star_w$ (where $x^\star_w$ marks the waterline) and (1.3) for $x<x^\star_w$. Notice that cell j is a typical almost dry cell and the use of the (first-order) piecewise constant reconstruction clearly leads to appearance of negative water depth values there. Indeed, in this cell the total amount of water is positive and therefore $\overline{w}_j>B_j$, but clearly $\overline{w}_j<B_{j+\frac{1}{2}}$ and thus $h_{j+\frac{1}{2}}<0$.

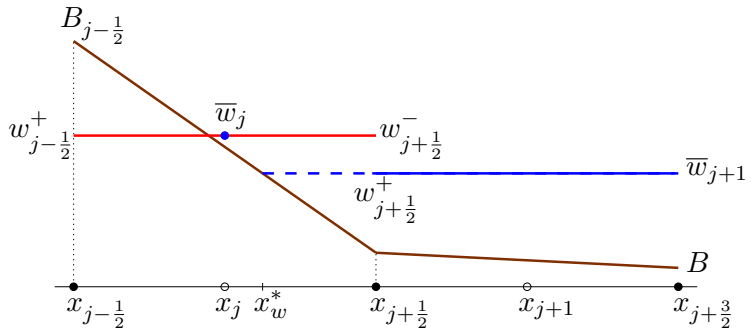

FIG. 3.1. *Wrong approximations of the wetting/drying front by the piecewise constant reconstruction.*

It is clear that replacement of the first-order piecewise constant reconstruction with a conventional second-order piecewise linear one will not guarantee positivity of the computed point values of h. Therefore, the reconstruction in cell j may need to be corrected. The correction proposed in [11] will solve the positivity problem by raising the water level at one of the cell edges to the level of the bottom function there and lowering the water level at the other edge by the same value (this procedure would thus preserve the amount of water in cell j). The resulting linear piece is shown in Figure 3.2. Unfortunately, as one may clearly see in the same figure, the obtained reconstruction is not well-balanced since the reconstructed values $w^-_{j+\frac{1}{2}}$ and $w^+_{j+\frac{1}{2}}$ are not the same.

Here, we propose an alternative correction procedure, which will be both positivity preserving and well-balanced even in the presence of dry areas. This correction bears some similarity to the reconstruction near dry fronts of depth-averaged granular avalanche models, which was proposed in [26]. However, in [26] the authors tracked a front running down the terrain, and thus did not have to treat well-balancing of equilibrium states.

Let us assume that at a certain time level all computed values $\overline{w}_j\geq B_j$ and the slopes $(\mathbf{U}_x)_j$ in the piecewise linear reconstruction (2.10) have been computed using some nonlinear limiter as it was discussed in §2 above. We also assume that at some

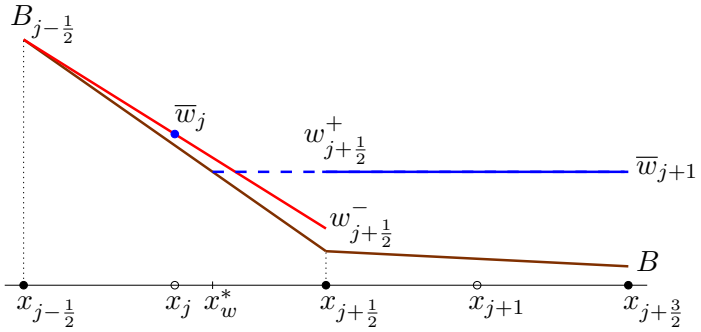

FIG. 3.2. *Approximations of the wetting/drying front by the positivity preserving but unbalanced piecewise linear reconstruction from [11].*

almost dry cell j,

$$B_{j+\frac{1}{2}} < \overline{w}_j < B_{j-\frac{1}{2}} \tag{3.1}$$

(the case $B_{j-\frac{1}{2}} < \overline{w}_j < B_{j+\frac{1}{2}}$ can obviously be treated in a symmetric way) and that the reconstructed values of w in cell $j+1$ satisfy $w^+_{j+\frac{1}{2}} > B_{j+\frac{1}{2}}, w^-_{j+\frac{3}{2}} > B_{j+\frac{3}{2}}$. This means that cell j is located near the dry boundary (mounting shore), and we design a well-balanced reconstruction correction procedure for cell j in the following way.

We begin by computing the free surface in cell j (denoted by w_j), which represents the average total water level in (*the flooded parts* of) this cell. The meaning of this formulation becomes clear from Figure 3.3. We always choose w_j such that the area enclosed between the line with height w_j and the bottom line equals the amount of water given by $\Delta x \cdot \overline{h}_j$, where $\overline{h}_j := \overline{w}_j - B_j$. The resulting area is either a trapezoid (if cell j is a fully flooded cell as in Figure 3.3 on the left) or a triangle (if cell j is a partially flooded cell as in Figure 3.3 on the right), depending on $\overline{h}_j$ and the bottom slope $(B_x)_j$.

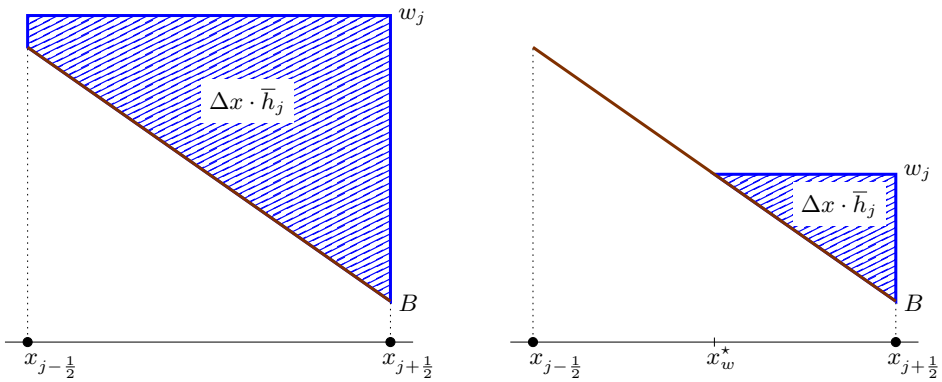

FIG. 3.3. Computation of w_j. Left: Fully flooded cell. Right: Partially flooded cell.

The precise definition is

$$w_j = \begin{cases} \overline{w}_j, & \text{if } \ \overline{h}_j \geq \frac{\Delta x}{2} \left|(B_x)_j\right|, \\ B_{j+\frac{1}{2}} + \Delta x_w^\star \left|(B_x)_j\right|, & \text{otherwise,} \end{cases} \tag{3.2}$$

where

$$\Delta x_w^\star = \left|x_{j+\frac{1}{2}} - x_w^\star\right|$$

and $x_w^\star$ is the boundary point that implicitly marks the waterline via the conservation of mass requirement

$$\frac{\Delta x_w^\star}{2}\left|B(x_w^\star) - B_{j+\frac{1}{2}}\right| = \Delta x \cdot \overline{h}_j,$$

which can be rewritten as

$$\frac{(\Delta x_w^\star)^2}{2}\left|(B_x)_j\right| = \Delta x \cdot \overline{h}_j,$$

and thus

$$\Delta x_w^\star = \sqrt{\frac{2\Delta x \overline{h}_j}{\left|(B_x)_j\right|}} = \sqrt{\frac{2\overline{h}_j}{\left|B_{j+\frac{1}{2}} - B_{j-\frac{1}{2}}\right|}}\ \Delta x. \tag{3.3}$$

Note that the limit for the distinction of cases in (3.2) is determined from the area of the triangle between the bottom line and the horizontal line at the level of $B_{j-\frac{1}{2}}$. We also note that if cell j satisfies (3.1), then it is clearly a partially flooded cell (like the one shown in Figure 3.3 on the right) with $\Delta x_w^\star < \Delta x$.

REMARK 3.1. *We would like to emphasize that if cell j is fully flooded, then the free surface is represented by the cell average $\overline{w}_j$ (see the first case in equation* (3.2)*), while if the cell is only partially flooded, $\overline{w}_j$ does not represent the free surface at all (see, e.g., Figure* 3.1*). Thus, in the latter case we need to represent the free surface with the help of another variable $w_j \neq \overline{w}_j$ (see the second case in* (3.2)*), which is only defined on the wet part of cell j, $[x_w^\star, x_{j+\frac{1}{2}}]$, and thus stays above the bottom function B, see Figure* 3.3 *(right).*

We now modify the the reconstruction in the partially flooded cell j to ensure well-balanced property. To this end, we first set $w^-_{j+\frac{1}{2}} = w^+_{j+\frac{1}{2}}$ (which immediately implies that $h^-_{j+\frac{1}{2}} := w^-_{j+\frac{1}{2}} - B_{j+\frac{1}{2}} = w^+_{j+\frac{1}{2}} - B_{j+\frac{1}{2}} =: h^+_{j+\frac{1}{2}}$) and determine the reconstruction of w in cell j via the conservation $\overline{h}_j$ in this cell. We distinguish between the following two possible cases. If the amount of water in cell j is sufficiently large (as in the case illustrated in Figure 3.4 on the left), we select $h^+_{j-\frac{1}{2}}$ to satisfy

$$\overline{h}_j = \frac{1}{2}(h^-_{j+\frac{1}{2}} + h^+_{j-\frac{1}{2}}), \tag{3.4}$$

obtain $w^+_{j-\frac{1}{2}} = h^+_{j-\frac{1}{2}} + B_{j-\frac{1}{2}}$, and thus the well-balanced reconstruction in cell j is completed.

If the value of $h^+_{j-\frac{1}{2}}$, computed from the conservation requirement (3.4) is negative, we replace a linear piece of w in cell j with two linear pieces as shown in Figure

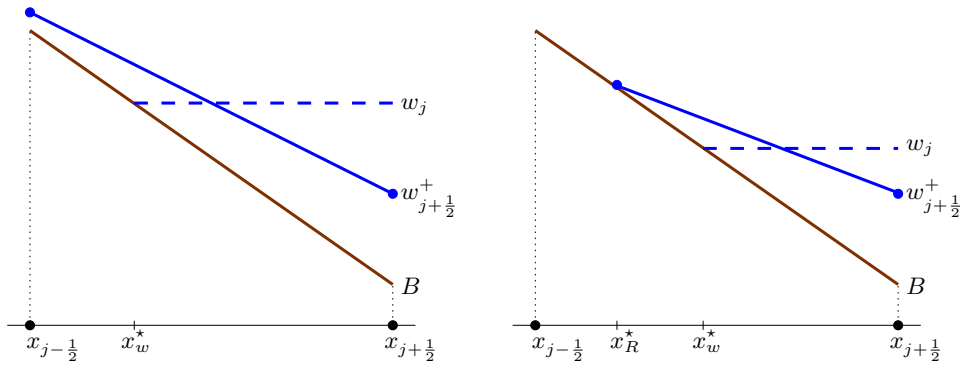

FIG. 3.4. Conservative reconstruction of w at the boundary with the fixed value $w^+_{j+\frac12}$. Left: Linear reconstruction with nonnegative $h^+_{j-\frac12}$. Right: Two linear pieces with $h^+_{j-\frac12}=0$.

3.4 on the right. The breaking point between the "wet" and "dry" pieces will be denoted by $x^\star_j$ and it will be determined from the conservation requirement, which in this case reads

$$\Delta x\cdot\overline{h}_j=\frac{\Delta x^\star_j}{2}h^-_{j+\frac12},\tag{3.5}$$

where

$$\Delta x^\star_R=\left|x_{j+\frac12}-x^\star_j\right|.$$

Combining the above two cases together, we obtain the reconstructed value

$$h^+_{j-\frac12}=\max\left\{0,2\overline{h}_j-h^-_{j+\frac12}\right\}.\tag{3.6}$$

We also generalize the definition of $\Delta x^\star_j$ and set

$$\Delta x^\star_j:=\Delta x\cdot\min\left\{\frac{2\overline{h}_j}{h^-_{j+\frac12}},1\right\},\tag{3.7}$$

which will be used in the proofs of the positivity and well-balancing of the resulting central-upwind scheme in §4.

REMARK 3.2. *In the beginning of this section, we assumed that the original reconstructed value of w at $x_{j+\frac12}$, obtained from the original piecewise linear reconstruction in cell $j+1$ satisfies the inequality $w^+_{j+\frac12}>B_{j+\frac12}$. If the latter is not true, we simply set $\Delta x^\star_j:=\Delta x^\star_w$ and $h^-_{j+\frac12}:=w_j-B_{j+\frac12}$. However, this situation is not generic and may occur only in the under-resolved computations.*

REMARK 3.3. *Notice that it may happen that at some cell j, $\overline{w}_j>B_{j+\frac12}$ and $\overline{w}_j>B_{j-\frac12}$, but either $w^-_{j+\frac12}<B_{j+\frac12}$ or $w^+_{j-\frac12}<B_{j-\frac12}$. In such a case, we are not at the situation of dry boundary (like the one depicted in Figure 1.1) and then the correction from [11] can be used without risking to produce an unbalance piecewise*

linear reconstruction. The linear piece in such cell j will be modified as follows:

$$\begin{aligned}
&\textit{If } \ w^-_{j+\frac12} < B_{j+\frac12}, \ \ \textit{then set } \ (w_x)_j := \frac{B_{j+\frac12} - \overline{w}_j}{\Delta x/2},\\
&\Longrightarrow \ \ w^-_{j+\frac12} = B_{j+\frac12}, \ \ w^+_{j-\frac12} = 2\overline{w}_j - B_{j+\frac12};
\end{aligned}$$

$$\begin{aligned}
&\textit{If } \ w^+_{j-\frac12} < B_{j-\frac12}, \ \ \textit{then set } \ (w_x)_j := \frac{\overline{w}_j - B_{j-\frac12}}{\Delta x/2},\\
&\Longrightarrow \ \ w^-_{j+\frac12} = 2\overline{w}_j - B_{j-\frac12}, \ \ w^+_{j-\frac12} = B_{j-\frac12}.
\end{aligned}$$

4. Positivity Preserving and Well-Balancing

In this section, we prove that the resulting central-upwind scheme is positivity preserving and well-balanced. For the positivity, our result is similar to the one proven in [11].

THEOREM 4.1. *Consider the system* (1.1) *and the semi-discrete central-upwind scheme* (2.5)–(2.14) *with the piecewise linear reconstruction* (2.10) *corrected according to the procedure described in §3. Assume that the system of ODEs* (2.5) *is solved by the forward Euler method and that for all j, $\overline{h}^n_j \ge 0$. Then, for all j, $\overline{h}^{n+1}_j \ge 0$, provided*

$$\Delta t \le \frac{1}{2a}\min_j\left\{\Delta x^\star_j\right\}, \qquad a := \max_j\left\{\max\{a^+_{j+\frac12}, -a^-_{j+\frac12}\}\right\}. \tag{4.1}$$

Proof: For the fully flooded cells with $\Delta x^\star_j = \Delta x$, the proof of Theorem 2.1 in [11] still holds. Therefore, we will only consider partially flooded cells like the one shown in Figure 3.4. First, from (3.5) we have that in such cell j the cell average of the water depth at time level $t = t^n$ is

$$\overline{h}^n_j = \frac{\Delta x^\star_j}{2\Delta x}\, h^-_{j+\frac12}, \tag{4.2}$$

and it is evolved to the next time level by applying the forward Euler temporal discretization to the first component of (2.5), which after the subtraction of the value B_j from the both sides can be written as

$$\overline{h}^{n+1}_j = \overline{h}^n_j - \lambda\left(\mathbf{H}^{(1)}_{j+\frac12} - \mathbf{H}^{(1)}_{j-\frac12}\right), \quad \lambda := \frac{\Delta t}{\Delta x}, \tag{4.3}$$

where the numerical fluxes are evaluated at time level $t = t^n$. Using (2.8) and the fact that by construction $w^+_{j+\frac12} - w^-_{j+\frac12} = h^+_{j+\frac12} - h^-_{j+\frac12}$, we obtain:

$$\mathbf{H}^{(1)}_{j+\frac12} = \frac{a^+_{j+\frac12}(hu)^-_{j+\frac12} - a^-_{j+\frac12}(hu)^+_{j+\frac12}}{a^+_{j+\frac12} - a^-_{j+\frac12}} + \frac{a^+_{j+\frac12}a^-_{j+\frac12}}{a^+_{j+\frac12} - a^-_{j+\frac12}}\left[h^+_{j+\frac12} - h^-_{j+\frac12}\right]. \tag{4.4}$$

Substituting (4.2) and (4.4) into (4.3) and taking into account the fact that in this cell $h^+_{j-\frac12} = 0$, we arrive at:

$$\begin{aligned}
\overline{h}^{n+1}_j = &\left[\frac{\Delta x^\star_j}{2\Delta x} - \lambda a^+_{j+\frac12}\left(\frac{u^-_{j+\frac12} - a^-_{j+\frac12}}{a^+_{j+\frac12} - a^-_{j+\frac12}}\right)\right] h^-_{j+\frac12}\\
&- \lambda a^-_{j+\frac12}\left(\frac{a^+_{j+\frac12} - u^+_{j+\frac12}}{a^+_{j+\frac12} - a^-_{j+\frac12}}\right) h^+_{j+\frac12} + \lambda a^+_{j-\frac12}\left(\frac{u^-_{j-\frac12} - a^-_{j-\frac12}}{a^+_{j-\frac12} - a^-_{j-\frac12}}\right) h^-_{j-\frac12},
\end{aligned} \tag{4.5}$$

Next, we argue as in [11, Theorem 2.1] and show that $\overline{h}_j^{n+1}$ is a linear combination of the three values, $h^{\pm}_{j+\frac{1}{2}}$ and $h^{-}_{j-\frac{1}{2}}$ (which are guaranteed to be nonnegative by our special reconstruction procedure) with nonnegative coefficients. To this end, we note that it follows from (2.13) and (2.14) that $a^{+}_{j+\frac{1}{2}} \geq 0$, $a^{-}_{j+\frac{1}{2}} \leq 0$, $a^{+}_{j+\frac{1}{2}} - u^{+}_{j+\frac{1}{2}} \geq 0$, and $u^{-}_{j+\frac{1}{2}} - a^{-}_{j+\frac{1}{2}} \geq 0$, and hence the last two terms in (4.5) are nonnegative. By the same argument, $0 \leq \frac{a^{+}_{j-\frac{1}{2}} - u^{+}_{j-\frac{1}{2}}}{a^{+}_{j-\frac{1}{2}} - a^{-}_{j-\frac{1}{2}}} \leq 1$ and $0 \leq \frac{u^{-}_{j+\frac{1}{2}} - a^{-}_{j+\frac{1}{2}}}{a^{+}_{j+\frac{1}{2}} - a^{-}_{j+\frac{1}{2}}} \leq 1$, and thus the first term in (4.5) will be also nonnegative, provided the CFL restriction (4.1) is satisfied. Therefore, $\overline{h}_j^{n+1} \geq 0$, and the proof is completed. □

Theorem 4.1 guarantees positivity of h, but the CFL timestep restriction (4.1) is quite severe since $\Delta x^{\star}_j$ may become arbitrarily small and then Δt would shrink. Our numerical experiments clearly demonstrate that the use of the theoretically small timesteps may slow down the computation to unacceptably large CPU times. We therefore adopt a strategy proposed in [2] which ensures positivity for general finite volume schemes.

We start by switching from the set of variables $\mathbf{U} = (w, hu)^T$ to the original variables $\mathbf{V} := (h, hu)^T$ in the ODE system (2.5) and discretize it using the forward Euler method, which leads to

$$\overline{\mathbf{V}}_j^{n+1} = \overline{\mathbf{V}}_j^{n} - \Delta t \left(\frac{\mathbf{H}_{j+\frac{1}{2}} - \mathbf{H}_{j-\frac{1}{2}}}{\Delta x} + \overline{\mathbf{S}}_j(t) \right). \tag{4.6}$$

We need to ensure that the first component of (4.6) satisfies

$$\overline{h}_j^{n+1} = \overline{h}_j^{n} - \Delta t \frac{\mathbf{H}^{(1)}_{j+\frac{1}{2}} - \mathbf{H}^{(1)}_{j-\frac{1}{2}}}{\Delta x} \geq 0. \tag{4.7}$$

Like in [2], we can then introduce the *draining time step*,

$$\Delta t_{j,\mathrm{drain}} = \frac{\Delta x \overline{h}_j^{n}}{\max(0, \mathbf{H}^{(1)}_{j+\frac{1}{2}}) + \max(0, -\mathbf{H}^{(1)}_{j-\frac{1}{2}})},$$

which describes the time when the water contained in cell j in the beginning of the time step has left via the outflow fluxes. We now replace the evolution step (4.7) with

$$\overline{h}_j^{n+1} = \overline{h}_j^{n} - \frac{\Delta t_{j+\frac{1}{2}} \mathbf{H}^{(1)}_{j+\frac{1}{2}} - \Delta t_{j-\frac{1}{2}} \mathbf{H}^{(1)}_{j-\frac{1}{2}}}{\Delta x},$$

where we set

$$\Delta t_{j+\frac{1}{2}} = \min(\Delta t, \Delta t_{i,\mathrm{drain}}), \quad i = j + \frac{1 - \mathrm{sgn}\left(\mathbf{H}^{(1)}_{j+\frac{1}{2}}\right)}{2}.$$

The definition of i selects the cell in upwind direction of the edge. The choice of $\Delta t_{j+\frac{1}{2}}$ guarantees the positivity of the water depth, which is also shown in [2, Theorem 4.1]. We would like to point out that the local modification of the time step only corresponds to the fact that the flux out of an empty cell vanishes, thus the physical flow is accurately represented here.

To ensure the well-balancing, we have to ensure that the gravity driven part of the flux is multiplied by the same time step as the source term. To this end, we follow [2] and split the flux (2.9) in its advective and gravity driven parts:

$$\mathbf{F}^{\mathrm{a}}(\mathbf{V}):=\left(hu,\frac{(hu)^2}{h}\right)^T \quad \text{and} \quad \mathbf{F}^{\mathrm{g}}(\mathbf{V}):=\left(0,\frac{g}{2}h^2\right)^T,$$

respectively. The corresponding advective and gravity driven parts of the central-upwind fluxes then read

$$\mathbf{H}^{\mathrm{g}}_{j+\frac12}(t)=\frac{a^+_{j+\frac12}\mathbf{F}^{\mathrm{g}}(\mathbf{V}^-_{j+\frac12})-a^-_{j+\frac12}\mathbf{F}^{\mathrm{g}}(\mathbf{V}^+_{j+\frac12})}{a^+_{j+\frac12}-a^-_{j+\frac12}}+\frac{a^+_{j+\frac12}a^-_{j+\frac12}}{a^+_{j+\frac12}-a^-_{j+\frac12}}\left[\mathbf{V}^+_{j+\frac12}-\mathbf{V}^-_{j+\frac12}\right],$$

and

$$\mathbf{H}^{\mathrm{a}}_{j+\frac12}(t)=\frac{a^+_{j+\frac12}\mathbf{F}^{\mathrm{a}}(\mathbf{V}^-_{j+\frac12})-a^-_{j+\frac12}\mathbf{F}^{\mathrm{a}}(\mathbf{V}^+_{j+\frac12})}{a^+_{j+\frac12}-a^-_{j+\frac12}},$$

as we chose to add the dissipation to $\mathbf{F}^{\mathrm{g}}$. The above fluxes adds up to the following modified finite volume update:

$$\overline{\mathbf{V}}^{n+1}_j=\overline{\mathbf{V}}^n_j-\left(\frac{\Delta t_{j+\frac12}\mathbf{H}^{\mathrm{a}}_{j+\frac12}-\Delta t_{j-\frac12}\mathbf{H}^{\mathrm{a}}_{j-\frac12}}{\Delta x}\right)-\Delta t\left(\frac{\mathbf{H}^{\mathrm{g}}_{j+\frac12}-\mathbf{H}^{\mathrm{g}}_{j-\frac12}}{\Delta x}+\overline{\mathbf{S}}^n_j\right). \tag{4.8}$$

This modification ensures the well-balancing property of the scheme even in the presence of dry areas, as we will show in Theorem 4.2.

REMARK 4.1. *The condition* (4.7) *is only violated close to the dry boundary. Away from these regions, we have* $\Delta t_{j+\frac12}=\Delta t$ *and therefore the finite volume updates* (4.8) *and* (4.6) *are almost the same.*

THEOREM 4.2. *Consider the system* (1.1) *and the fully discrete central-upwind scheme* (4.8). *Assume that the numerical solution* $\mathbf{V}(t^n)$ *corresponds to the steady state which is a combination of the "lake at rest"* (1.2) *and "dry lake"* (1.3) *states in the sense that for all* w_j *defined in* 3.2, $w_j=\mathrm{Const}$ *and* $u=0$ *whenever* $h_j>0$. *Then* $\mathbf{V}(t^{n+1})=\mathbf{V}(t^n)$, *that is, the scheme is* well-balanced.

Proof: We have to show that in all cells the fluxes and the source term discretization cancel exactly. First, we mention the fact that the reconstruction procedure derived in §3 preserves both the "lake at rest" and "dry lake" steady states and their combinations. For all cells where the original reconstruction is not corrected, the resulting slopes are obviously zero and therefore $w^{\mp}_{j\pm\frac12}=w_j$ there. As $hu=0$ in all cells, the reconstruction for hu obviously reproduces the constant point values $(hu)^{\mp}_{j\pm\frac12}=0$, $\forall j$.

Now we analyze the fluxes $\mathbf{H}^{\mathrm{a}}_{j+\frac12}$ and $\mathbf{H}^{\mathrm{g}}_{j+\frac12}$ from (4.8). The first component is

$$\mathbf{H}^{\mathrm{a},(1)}_{j+\frac12}+\mathbf{H}^{\mathrm{g},(1)}_{j+\frac12}=\frac{a^+_{j+\frac12}(hu)^-_{j+\frac12}-a^-_{j+\frac12}(hu)^+_{j+\frac12}}{a^+_{j+\frac12}-a^-_{j+\frac12}}+\frac{a^+_{j+\frac12}a^-_{j+\frac12}}{a^+_{j+\frac12}-a^-_{j+\frac12}}\left[h^+_{j+\frac12}-h^-_{j+\frac12}\right]=0,$$

as $h^+_{j+\frac12}=h^-_{j+\frac12}$ and $(hu)^+_{j+\frac12}=(hu)^-_{j+\frac12}=0$. Using the same argument and setting $u^{\pm}_{j+\frac12}=0$ at the points $x=x_{j+\frac12}$ where $h^+_{j+\frac12}=h^-_{j+\frac12}=0$, for the second component we

obtain

$$\mathbf{H}^{\mathrm{a},(2)}_{j+\frac{1}{2}}+\mathbf{H}^{\mathrm{g},(2)}_{j+\frac{1}{2}}=\frac{a^+_{j+\frac{1}{2}}\left(hu^2\right)^-_{j+\frac{1}{2}}-a^-_{j+\frac{1}{2}}\left(hu^2\right)^+_{j+\frac{1}{2}}}{a^+_{j+\frac{1}{2}}-a^-_{j+\frac{1}{2}}}+\frac{a^+_{j+\frac{1}{2}}\left(\frac{g}{2}h^2\right)^-_{j+\frac{1}{2}}-a^-_{j+\frac{1}{2}}\left(\frac{g}{2}h^2\right)^+_{j+\frac{1}{2}}}{a^+_{j+\frac{1}{2}}-a^-_{j+\frac{1}{2}}}$$
$$+\frac{a^+_{j+\frac{1}{2}}a^-_{j+\frac{1}{2}}}{a^+_{j+\frac{1}{2}}-a^-_{j+\frac{1}{2}}}\left[(hu)^+_{j+\frac{1}{2}}-(hu)^-_{j+\frac{1}{2}}\right]=\frac{g}{2}h^2_{j+\frac{1}{2}},$$

where $h_{j+\frac{1}{2}}:=h^+_{j+\frac{1}{2}}=h^-_{j+\frac{1}{2}}$. So, the finite volume update (4.8) for the studied steady state reads

$$\overline{\mathbf{V}}^{n+1}_j=\overline{\mathbf{V}}^n_j-\frac{\Delta t}{\Delta x}\begin{bmatrix}0\\ \frac{g}{2}h^2_{j+\frac{1}{2}}-\frac{g}{2}h^2_{j-\frac{1}{2}}\end{bmatrix}+\Delta t\overline{\mathbf{S}}^n_j. \tag{4.9}$$

After substituting the source quadrature (2.7) into (4.9), it remains to show that for all j,

$$\frac{h^2_{j+\frac{1}{2}}-h^2_{j-\frac{1}{2}}}{2}=-\overline{h}^n_j\left(B_{j+\frac{1}{2}}-B_{j-\frac{1}{2}}\right). \tag{4.10}$$

We now check (4.10) in the two possible cases. In the fully flooded cells, where $w_j>B_{j\pm\frac{1}{2}}$, we have

$$\frac{h^2_{j+\frac{1}{2}}-h^2_{j-\frac{1}{2}}}{2}=\frac{h_{j+\frac{1}{2}}+h_{j-\frac{1}{2}}}{2}\left(h_{j+\frac{1}{2}}-h_{j-\frac{1}{2}}\right)=\overline{h}^n_j\left(w_j-B_{j+\frac{1}{2}}-w_j+B_{j-\frac{1}{2}}\right)$$
$$=-\overline{h}^n_j\left(B_{j+\frac{1}{2}}-B_{j-\frac{1}{2}}\right),$$

and thus (4.10) is satisfied. In the partially flooded cells (as the one shown in Figure 3.3 on the right), $w_j<B_{j-\frac{1}{2}}$, $h_{j-\frac{1}{2}}=0$, and thus using (3.5) equation (4.10) reduces to

$$\frac{h^2_{j+\frac{1}{2}}}{2}=-\frac{\Delta x^\star_j h_{j+\frac{1}{2}}}{2\Delta x}\left(B_{j+\frac{1}{2}}-B_{j-\frac{1}{2}}\right)=-\frac{h_{j+\frac{1}{2}}}{2}\Delta x^\star_j(B_x)_j,$$

which is true since at the studied-steady situation, $x^\star_j=x^\star_w$, which implies that $\Delta x^\star_j=\Delta x^\star_w$, and hence, $-\Delta x^\star_j(B_x)_j=h_{j+\frac{1}{2}}$ (see Figure 3.3 (right)).

This concludes the proof of the theorem. □

Remark 4.2. *We would like to point out that the resulting scheme will clearly remain positivity preserving if the forward Euler method in the discretization of the ODE system* (2.5) *is replaced with a higher-order SSP ODE solver (either the Runge-Kutta or the multistep one), because such solvers can be written as a convex combination of several forward Euler steps, see [5].*

5. Numerical Experiments

Like in [11], we set $\theta=1.3$ in the minmod function (2.11). The time step for our computations is adaptively set to

$$\Delta t=\mu\frac{\Delta x}{a},\qquad a=\max_j\left\{\max(a^+_{j+\frac{1}{2}},-a^-_{j+\frac{1}{2}})\right\},$$

and the CFL number is set to $\mu=0.5$.

To show the effects of our new reconstruction at the boundary, we compare our new scheme with the scheme from [11]. These schemes only differ in the treatment of the dry boundary, so that the effects of the proposed modifications are highlighted. For the sake of brevity, we refer to the scheme from [11] as KP and to our new scheme as BKN.

5.1. Oscillating Lake

In this section, we consider present a test case proposed in [1]. It describes the situation where the "lake at rest" (1.2) and "dry lake" (1.3) are combined in the domain $[0,1]$ with the bottom topography given by

$$B(x)=\frac{1}{4}-\frac{1}{4}\cos((2x-1)\pi), \tag{5.1}$$

and the following initial data:

$$h(x,0)=\max(0,0.4-B(x)), \qquad u(x,0)\equiv 0. \tag{5.2}$$

We compute the numerical solution by the KP and BKN schemes with $\Delta x=0.005$ at the final time $T=19.87$. The results are shown in Figure 5.1. As one can clearly see there, the KP scheme introduces small oscillations at the boundary, whereas the BKN scheme is perfectly well-balanced. The errors measured in both the L^∞- and L^1-norms are given in Table 5.1.

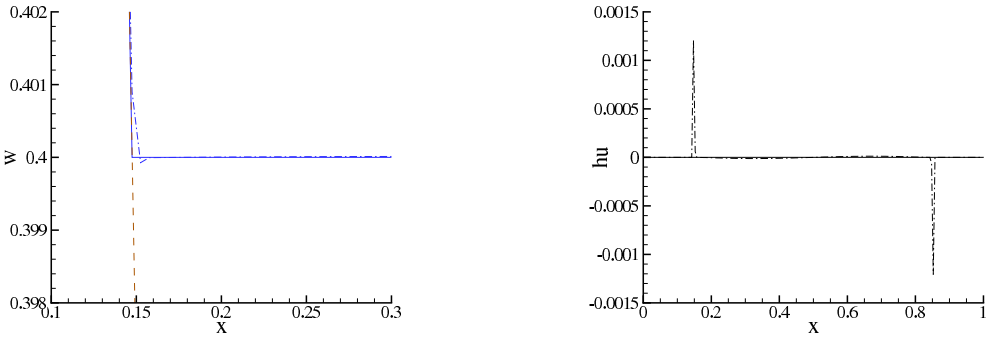

FIG. 5.1. *Lake at rest. Left: Zoom on free surface. Right: Discharge. BKN scheme (solid line), KP scheme (dash-dotted line) and bottom topography (dashed line).*

	h		hu	
Scheme	L^∞-error	L^1-error	L^∞-error	L^1-error
KP	7.1305e-04	1.5901e-05	1.2071e-03	1.7757e-05
BKN	9.4258e-14	6.5084e-14	2.1373e-15	8.3680e-16

TABLE 5.1. *Errors in the computation of the steady state.*

We now consider a sinusoidal perturbation of the steady state (5.1), (5.2) by taking

$$h(x,0)=\max\left(0,0.4+\frac{\sin(4x-2-\max(0,-0.4+B(x)))}{25}-B(x)\right).$$

As in [1], we set the final time to be $T=19.87$. At this time, the wave has its maximal height at the left shore after some oscillations.

In Figure 5.2 we compare the results obtained by the BKN and KP schemes used with $\Delta x=0.005$. One can clearly see that the new scheme produces a significantly higher run-up on the shore, thus the oscillation is less damped. For the discharge, the BKN scheme produces no oscillations at the boundary. As the overshoots of the KP scheme are directed downslope, this could be the reason for the reduced run-up. It is surprising that our modifications, which only affect the water height, have such an impact on the discharge as well.

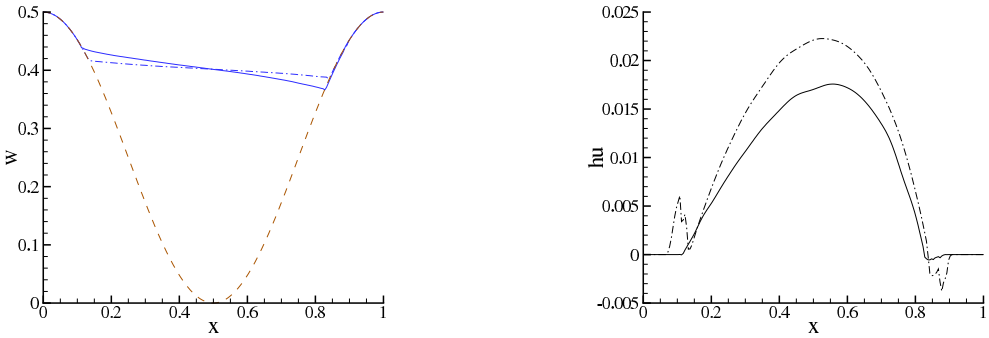

FIG. 5.2. *Oscillating lake. Left: Free surface and bottom topography. Right: Discharge. BKN scheme (solid line), KP scheme (dash-dotted line) and bottom topography (dashed line)*

Tables 5.2 and 5.3 show the experimental convergence rates for the two different schemes. While none of the schemes reaches their formal second order in this example, the convergence rates of the BKN scheme are clearly better. This is especially true for the discharge, where the error of the KP scheme does not reduce for the finest grids.

# points	h error	EOC	hu error	EOC
25	1.43e-02		9.75e-03	
50	1.04e-02	0.46	8.33e-03	0.23
100	6.38e-03	0.71	3.39e-03	1.30
200	3.48e-03	0.88	1.66e-03	1.02
400	1.31e-03	1.41	1.38e-03	0.27
800	7.21e-04	0.86	8.84e-04	0.64

TABLE 5.2. *Oscillating lake: Experimental order of convergence (EOC) for the BKN scheme. The errors are measured in the L^1-norm; the reference solution was computed using 3200 grid cells.*

5.2. Wave Run-Up on a Sloping Shore

This test describes the run-up and reflection of a wave on a mounting slope. It was proposed in [25] and reference solutions can be found, for example, in [2, 19].

The initial data are

$$H_0(x)=\max\left\{D+\delta\,\mathrm{sech}^2(\gamma(x-x_a)),B(x)\right\},\qquad u_0(x)=\sqrt{\frac{g}{D}}H_0(x),$$

# points	h error	EOC	hu error	EOC
25	1.26e-02		1.67e-02	
50	1.62e-02	-0.36	1.12e-02	0.58
100	1.21e-02	0.42	2.23e-03	2.33
200	9.71e-03	0.32	2.44e-03	-0.13
400	6.67e-03	0.54	2.74e-03	-0.16
800	3.77e-03	0.82	2.73e-03	0.01

TABLE 5.3. *Oscillating lake: Experimental order of convergence (EOC) for the KP scheme. The errors are measured in the L^1-norm; the reference solution was computed by the BKN scheme using 3200 grid cells.*

and the bottom topography is

$$B(x)=\begin{cases}0, & \text{if } x<2x_a,\\ \dfrac{x-2x_a}{19.85}, & \text{otherwise.}\end{cases}$$

As in [2, 19], we set

$$D=1,\quad \delta=0.019,\quad \gamma=\sqrt{\frac{3\delta}{4D}},\quad x_a=\sqrt{\frac{4D}{3\delta}}\operatorname{arccosh}\bigl(\sqrt{20}\bigr).$$

The computational domain is $[0,80]$ and the grid size $\Delta x=0.04$.

In Figures 5.3 and 5.4, we present the free surface and discharge of the solutions computed by both BNK and KP schemes (dash-dotted lines) for different times t. The numerical solutions are compared with the exact solution (solid line). Details on how to obtain the analytical solution can be found in [24, Section 3.5.2]. Both schemes provide accurate solutions which compare very well with the exact one. While for the free surface a difference is barely visible, the new BKN scheme gives a slightly smoother solution for the discharge—the disturbances at the dry boundary are less pronounced. The difference becomes more visible when the solution returns to the the lake at rest state at $t=80$. At this time, the discharge computed by the KP scheme is roughly three times as big as the one obtained by the BKN scheme, although both values are relatively small.

Acknowledgment. The first ideas for this work were discussed by the authors at a meeting at the "Mathematisches Forschungsinstitut Oberwolfach". The authors are grateful for the support and inspiring atmosphere there. The research of A. Kurganov was supported in part by the NSF Grant DMS-0610430. The research of A. Bollermann and S. Noelle was supported by DFG Grant NO361/3-1.

REFERENCES

[1] E. Audusse, F. Bouchut, M.-O. Bristeau, R. Klein and B. Perthame, *A fast and stable well-balanced scheme with hydrostatic reconstruction for shallow water flows*, SIAM J. Sci. Comput., 25, 2050-2065, 2004.

[2] A. Bollermann, S. Noelle and M. Lukáčová-Medvid'ová, *Finite volume evolution Galerkin methods for the shallow water equations with dry beds*, accepted for publication in Commun. Comput. Phys., 2010.

[3] T. Gallouët, J.-M. Hérard and N. Seguin, *Some approximate Godunov schemes to compute shallow-water equations with topography*, Comput. & Fluids, 32, 479-513, 2003.

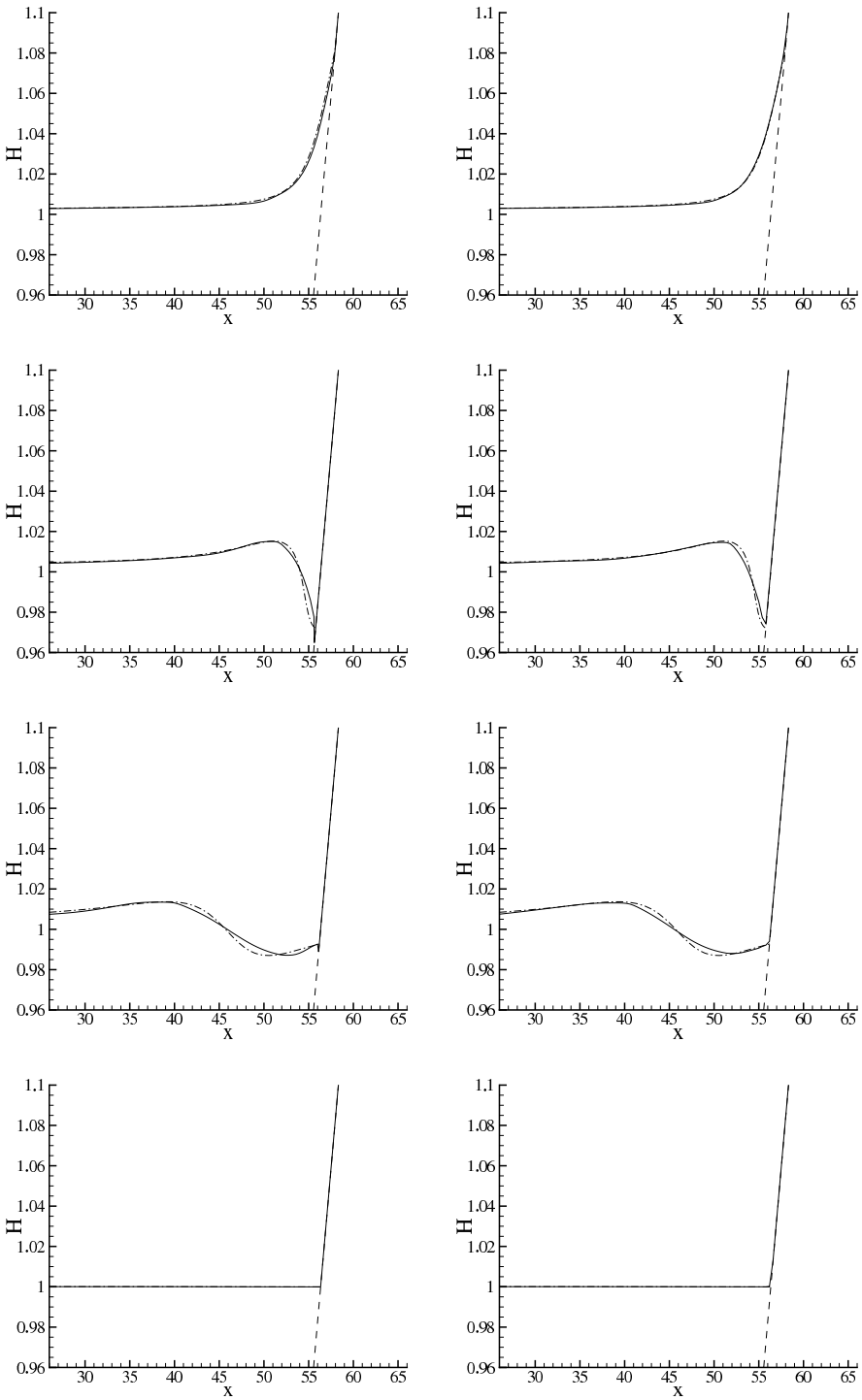

FIG. 5.3. *Wave run-up on a sloping shore, free surface and bottom line. Left: BKN scheme. Right: KP scheme. From top to bottom:* $t = 17, 23, 28, 80$.

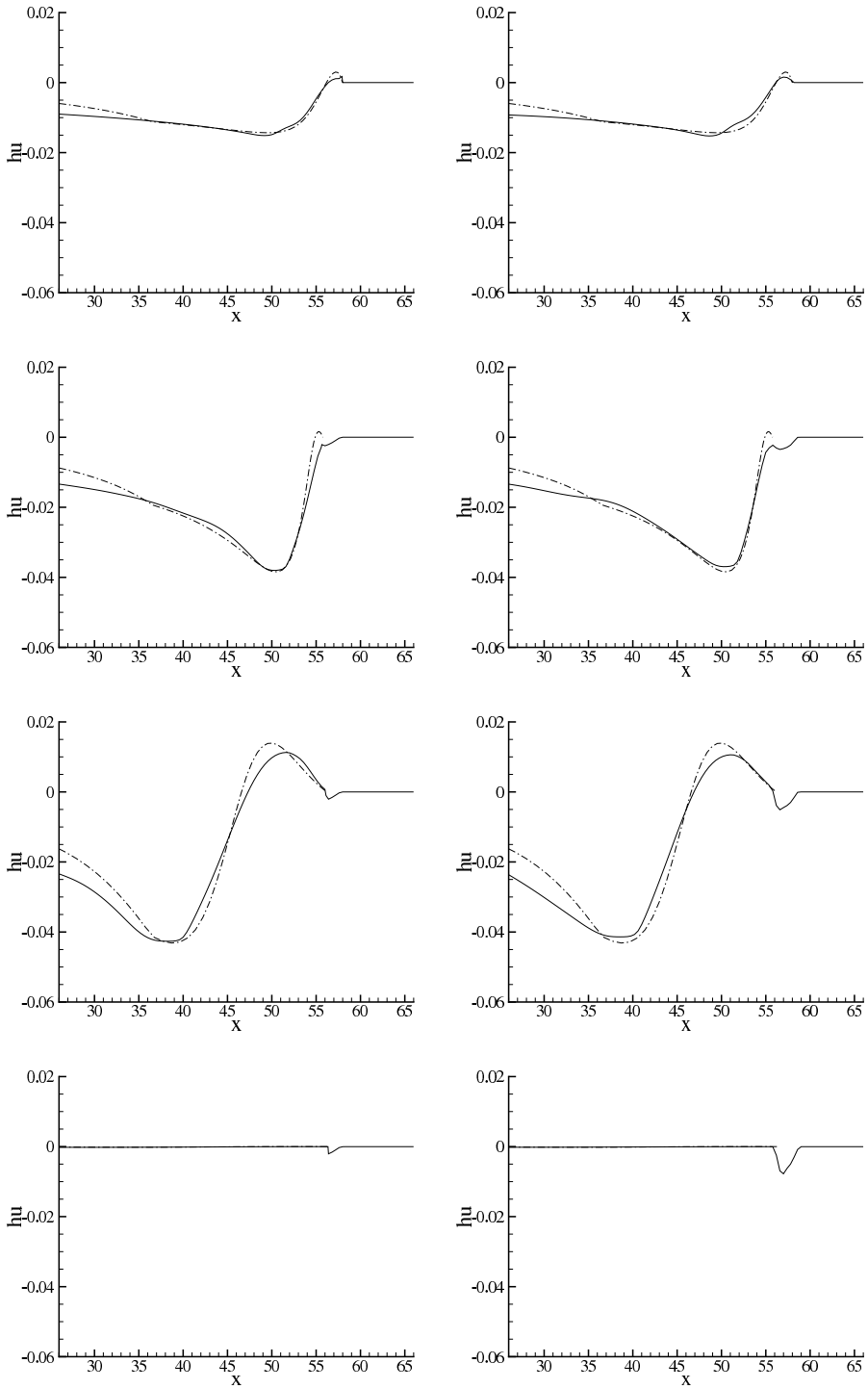

FIG. 5.4. *Wave run-up on a sloping shore, discharge. Left: BKN scheme. Right: KP scheme. From top to bottom:* $t = 17, 23, 28, 80$.

[4] E. Godlewski and P.-A. Raviart, *Numerical approximation of hyperbolic systems of conservation laws*, Springer-Verlag, New York, 1996.
[5] S. Gottlieb, C.-W. Shu and E. Tadmor, *High order time discretization methods with the strong stability property*, SIAM Review, 43, 89-112, 2001.
[6] S. Jin, *A steady-state capturing method for hyperbolic system with geometrical source terms*, M2AN Math. Model. Numer. Anal., 35, 631-645, 2001.
[7] S. Jin and X. Wen, *Two interface-type numerical methods for computing hyperbolic systems with geometrical source terms having concentrations*, SIAM J. Sci. Comput., 26, 2079-2101, 2005.
[8] D. Kröner, *Numerical Schemes for Conservation Laws*, Wiley, Chichester, 1997.
[9] A. Kurganov and D. Levy, *Central-upwind schemes for the Saint-Venant system*, M2AN Math. Model. Numer. Anal., 36, 397-425, 2002.
[10] A. Kurganov, S. Noelle and G. Petrova, *Semi-discrete central-upwind schemes for hyperbolic conservation laws and Hamilton-Jacobi equations*, SIAM J. Sci. Comput., 23, 707-740, 2001.
[11] A. Kurganov and G. Petrova, *A second-order well-balanced positivity preserving central-upwind scheme for the Saint-Venant system*, Commun. Math. Sci., 5(1):133–160, 2007.
[12] B. van Leer, *Towards the ultimate conservative difference scheme, V. A second order sequel to Godunov's method*, J. Comput. Phys., 32, 101-136, 1979.
[13] R.J. LeVeque, *Balancing source terms and flux gradients in high-resolution Godunov methods: the quasi-steady wave-propagation algorithm*, J. Comput. Phys., 146, 346-365, 1998.
[14] R. LeVeque, *Finite volume methods for hyperbolic problems*, Cambridge Texts in Applied Mathematics, Cambridge University Press, 2002.
[15] K.-A. Lie and S.Noelle, *On the artificial compression method for second-order nonoscillatory central difference schemes for systems of conservation laws*, SIAM J. Sci. Comput., 24, 1157-1174, 2003.
[16] H. Nessyahu and E. Tadmor, *Non-oscillatory central differencing for hyperbolic conservation laws*, J. Comput. Phys., 87, 408-463, 1990.
[17] S. Noelle, N. Pankratz, G. Puppo and J. Natvig, *Well-balanced finite volume schemes of arbitrary order of accuracy for shallow water flows*, J. Comput. Phys., 213, 474-499, 2006.
[18] B. Perthame and C. Simeoni, *A kinetic scheme for the Saint-Venant system with a source term*, Calcolo, 38, 201-231, 2001.
[19] M. Ricchiuto and A. Bollermann, *Stabilized residual distribution for shallow water simulations*, Journal of Computational Physics, 228:1071–1115, 2009.
[20] G. Russo, *Central schemes for balance laws*. Hyperbolic problems: theory, numerics, applications, Vol. I, II (Magdeburg, 2000), 821-829, Internat. Ser. Numer. Math., 140, 141, Birkhäuser, Basel, 2001.
[21] G. Russo, *Central schemes for conservation laws with application to shallow water equations*, in Trends and applications of mathematics to mechanics: STAMM 2002, S. Rionero and G. Romano (eds.), 225–246, Springer-Verlag Italia SRL, 2005.
[22] A.J.C. de Saint-Venant, *Théorie du mouvement non-permanent des eaux, avec application aux crues des rivière at à l'introduction des warées dans leur lit*, C.R. Acad. Sci. Paris, 73, 147-154, 1871.
[23] P. K. Sweby, *High resolution schemes using flux limiters for hyperbolic conservation laws*, SIAM J. Numer. Anal., 21, 995-1011, 1984.
[24] C. E. Synolakis. *The runup of long waves*. PhD thesis, California Institute of Technology, 1986.
[25] C. E. Synolakis, *The runup of solitary waves*, J. Fluid Mech. 185, 523–545, 1987.
[26] Y. C.Tai, S. Noelle, J. M. N. T. Gray, K. Hutter *Shock-Capturing and Front-Tracking Methods for Granular Avalanches*, J. Comput. Phys. 175, 269–301, 2002.
[27] Y. Xing and C.-W. Shu, *High order finite difference WENO schemes with the exact conservation property for the shallow water equations*, J. Comput. Phys., 208, 206-227, 2005.
[28] Y. Xing and C.-W. Shu, *A new approach of high order well-balanced finite volume WENO schemes and discontinuous Galerkin methods for a class of hyperbolic systems with source terms*, Commun. Comput. Phys., 1, 100-134, 2006.